Phase Transitions in Asymmetric Rod−Coil Block Copolymers

Bradley D. Olsen and Rachel A. Segalman*

Department of Chemical Engineering, University of California Berkeley, Berkeley, California 94720, and Materials Science Division, Lawrence Berkeley Laboratory

Received May 3, 2006; Revised Manuscript Received July 9, 2006

ABSTRACT: Poly(alkoxyphenylenevinylene-*b*-isoprene) is used to study the phase transitions of a weakly segregated rod−coil block copolymer system. In the high coil fraction region of the phase diagram, phase transitions are caused by relatively small changes in temperature and composition. Several different sequences of phase transitions are observed, allowing fine control of structure, orientation, and thermal history effects. Weakly segregated symmetric rod−coil block copolymers organize into lamellar microphases at low temperature and disorder into nematic and isotropic phases with increasing temperature. As the coil fraction is increased, the lamellar structure loses long-range order but the microphase structure does not change. In these asymmetric block copolymers, a distinct change in phase transitions upon heating is observed. The stable nematic window narrows as the coil fraction increases. As a result, while symmetric block copolymers transition from a lamellar to an intermediate nematic and finally to an isotropic phase upon heating, coil-rich block copolymers transition is directly from a lamellar to an isotropic. The division between these two regimes occurs at a coil fraction of ~0.8.

Introduction

The application of many functional rodlike polymers, such as conjugated polymers and helical polypeptides, requires control over their nanoscale structure. For example, in organic electronics, devices incorporate multiple polymeric components to promote balanced charge transport, exciton recombination, or charge separation. Controlling the structure of the conjugated polymer phases and the internal interfaces between them on the 10 nm length scale of exciton diffusion is crucial.[1,2] Block copolymers present an attractive method for structural control by self-assembling into a variety of nanostructured phases.[3−6] While most research has focused on coil−coil block copolymers, functional rod−coil block copolymers have also been synthesized, though their self-assembly behavior is less well studied.[7−11] In these materials the interplay between various segmental interactions and geometric effects creates unique phase behavior that includes both nanoscale phase separation and liquid crystallinity. Similarly to coil−coil block copolymers, the phase behavior of rod−coil materials is governed by the Flory−Huggins interaction and the volume fraction of the two blocks. Additionally, liquid crystalline interactions between the rodlike polymers, parametrized by a Maier−Saupe parameter, and a geometric factor to account for the conformational asymmetry between the rod and coil are necessary to characterize the system.[12,13] Since phase space in a rod−coil block copolymer system is characterized by four parameters as compared to the two in coil−coil systems, these systems demonstrate novel equilibrium thermodynamics, and the creation of a universal phase diagram is unusually complex.

We recently reported one of the first phase diagrams for a model rod−coil system based on poly(alkoxyphenylenevinylene) (PPV) rods and polyisoprene (PI) coils.[14] A dense coat of side chains on the PPV rod moderates the rod−rod and rod−coil interactions, resulting in a system that maintains its thermal processability and miscibility at polymeric molecular weights. As a result, the order to microphase disorder transition (ODT) and the liquid crystalline clearing temperature were both accessible. The phase diagram showed regions of stable isotropic, nematic, and lamellar phases, and the shape of the diagram agreed qualitatively with the results of Landau calculations[15] and SCFT theory.[12,13] However, the nature of the disordering transition in the asymmetric rod−coil block copolymers was unclear. For block copolymers with long coils, the nematic−isotropic transition temperature decreases rapidly with increasing coil fraction and the width of the nematic region narrows. Calculations based on Landau theories suggest that at high enough coil fractions lamellar and isotropic regions will persist, but there may be a region without a stable nematic phase.[15,16] SCFT calculations assuming perfect rod alignment predict qualitatively similar ODT behavior as the Landau calculations,[13] and in calculations where the rod alignment is allowed to vary the nematic phase also ceases to exist at high enough coil fractions.[12] The existence of these distinct ordered−nematic−isotropic and ordered−isotropic phase transition sequences, illustrated in Figure 1, would have a significant impact on thermal history and ordering in these materials. At high coil fractions the ODT temperature also decreases rapidly, and the steep slope of the ODT curve in the asymmetric region implies that transitions can be accessed by small changes in composition. The ability to use small changes in temperature or block copolymer composition to achieve control over molecular order and orientation in the asymmetric region of the phase diagram can provide a powerful tool for control of order and orientation in functional rod−coil materials.

While only lamellar structures have been observed in studies of the weakly segregated PPV-*b*-PI system,[14,17] studies of other rod−coil materials have shown a variety of phases, including lamellar and hexagonal phases in rod−coil block copolypeptides[7,18−22] and zigzag, arrowhead, wavy lamellar,[23,24] and smectic A-like lamellae[25] in high molecular weight systems. Hexagonal strip and puck phases have been reported in asymmetric rod−coil oligomers,[26−33] and certain oligomers also exhibited disordering transitions.[26,27,29−31] However, in many oligomeric structures the coil block is fully extended, resulting in a breakdown of polymeric scaling behavior. The PPV-*b*-PI system, with its processability and accessible transitions, is a useful polymeric

* Corresponding author: e-mail segalman@berkeley.edu.

10.1021/ma060994z CCC: $33.50
Published on Web 09/12/2006

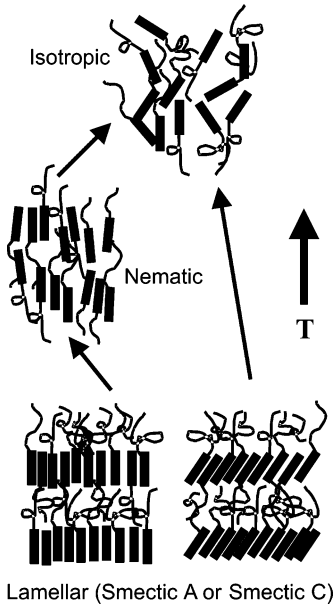

Figure 1. Schematic of disordering phase transitions in rod−coil block copolymers. Weakly segregated PPV-*b*-PI block copolymers show two types of phase transition behavior. Symmetric and slightly asymmetric polymers exhibit a low-temperature lamellar phase, followed by nematic and then isotropic phases with increasing temperature. Polymers with very high coil fractions (near the order−disorder composition) proceed through a direct transition from the lamellar to the isotropic phase with increasing temperature.

system in which to probe the effect of volume fraction asymmetry on equilibrium structure.

This study investigates the relative stability of the ordered, nematic, and isotropic phases and the thermodynamic transitions in liquid crystalline ordering in asymmetric rod−coil block copolymers. A series of PPV-*b*-PI copolymers are prepared across a narrow range of coil fractions, and we establish that the lamellar phase is stable across the entire ordered region of the phase diagram. We also identify two regions characterized by separate series of liquid crystalline transitions: one from the lamellar to nematic to isotropic phases and a second directly from the lamellar to isotropic phase.

Experimental Methods

Synthesis. Synthesis of poly(2,5-di(2′-ethylhexyloxy)-1,4-phenylenevinylene) (DEH−PPV) was carried out as described previously.[14] Siegrist polycondensation[11,34] was chosen as the polymerization technique because it allows low-polydispersity PPV to be produced with few chemical defects in the polymer backbone. The PPV homopolymer showed a transition from a solid to liquid crystalline phase at 57 °C by differential scanning calorimetry and a liquid crystalline clearing temperature at 194 °C by polarized optical microscopy. Poly(1,4-isoprene) (PI) was synthesized anionically in a nonpolar solvent to achieve 93% 1,4-addition and quenched with PPV to form the block copolymer, as described previously.[14] Scheme 1 illustrates the chemical structure of the final block copolymer.

Molecular Weight Determination. Molecular weights were measured on a Waters 2690 gel permeation chromatograph (GPC) with a Viscotek refractive index detector and a low-angle light scattering detector using a 670 nm laser. Light scattering was used for absolute molecular weight determination without the use of calibration standards for the polyisoprene blocks, and the polydispersity of all PI samples was less than 1.05. The number-average molecular weight of the PPV block was also measured by NMR end-group analysis, and the polydispersity was estimated to be 1.17 using polystyrene standards. Because of the complex hydrodynamics of rodlike molecules,[35,36] this polydispersity represents an upper limit on the true PPV polydispersity. The hydrodynamic volume of the rod molecules increases much more rapidly with molecular weight than the hydrodynamic volume of coil polymers, effectively stretching the high molecular weight tail of the distribution in rod polymers and increasing the apparent polydispersity calculated on the basis of coil polymer standards. Molecular weights for each block are shown in Table 1. N is the number of volumetric repeat units in each block copolymer (one PI monomer is used as a reference volume), and ϕ is the volume fraction of PI. Rod and coil dimensions were calculated on the basis of bond length and density data as described previously[14] and are given in Table 1. The coil to rod length ratio, ν, is related to the geometric parameter used in self-consistent field theories.[12,13]

Scheme 1. Structure of PPV-*b*-PI Rod−Coil Block Copolymers

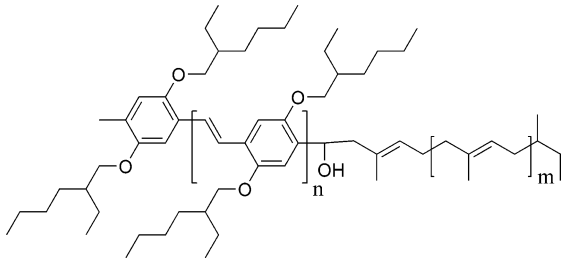

Characterization. Samples for small-angle X-ray scattering (SAXS) were prepared by annealing polymers in a vacuum oven at 120 °C for 24 h to form 1 mm thick disks and then sealing the sample between Kapton windows. Experiments were performed on beamline 1-4 of the Stanford Synchrotron Radiation Laboratory (SSRL). The beamline was configured with an X-ray wavelength of 1.488 Å and focused to a spot size of ∼0.5 mm diameter. Data were converted to absolute intensities as described previously.[14] Samples for transmission electron microscopy (TEM) were prepared by spin-coating films of ∼100 nm thickness from 2% toluene solution onto silicon nitride windows. All samples were annealed under vacuum at room temperature for 12 h. Polymers were stained by exposure to the vapor from a 2% OsO_4 solution for 3 h. Bright-field images were taken immediately after staining on a JEOL 200CX microscope at the National Center for Electron Microscopy operating at an accelerating voltage of 200 kV.

The liquid crystalline behavior of the samples was investigated through polarized optical microscopy (POM) and depolarized light scattering (DPLS). An Olympus BX51 microscope with crossed polarizers and an Instec HCS302 heat stage were used to image samples, as previously described.[14] The liquid crystalline clearing temperature (transition to the isotropic phase) is identified as the point at which the sample loses all optical texture under crossed polarizers. Samples for DPLS were prepared by annealing a sample of polymer at 80 °C overnight in a vacuum oven to form an ∼0.1 mm thick disk and then sealing the sample between two quartz windows. Depolarized light scattering was measured using a previously described instrument.[37] The sample was heated and cooled three times, and data to determine transitions were taken from the first cooling and second heating passes. Reported values of I/I_0 were normalized by the transmission of the sample. The transition to the isotropic phase was identified as the point at which the DPLS signal dropped to the baseline level.

Results and Analysis

Structure of Asymmetric Rod−Coil Block Copolymers. Only lamellar ordered phases, as identified by the combination of small-angle scattering and electron microscopy, are observed in the weakly segregated polymeric PPV-*b*-PI system. SAXS spectra for all polymers, shown in Figure 2, demonstrate peaks at q^* and $2q^*$ characteristic of lamellar structure. At low coil fractions, a well-ordered lamellar structure is observed through TEM micrographs in Figure 3 and sharp Bragg peaks in Figure 2. As the coil fraction is increased, a decrease in long-range order is observed in TEM micrographs. Additionally, the two

Table 1. Molecular Weight and Characteristic Dimensions of PPV-*b*-PI Rod−Coil Block Copolymers

block copolymer	PPV M_n (g/mol)	PI M_n (g/mol)	N	ϕ	ν	rod length (nm)	coil R_g (nm)	block copolymer contour length (nm)
PPVbPI-67	3400	6300	138	0.67	0.417	6.15	2.57	47.9
PPVbPI-77	3400	10300	197	0.77	0.534	6.15	3.28	74.3
PPVbPI-82	3400	13900	249	0.82	0.620	6.15	3.80	97.5
PPVbPI-85	3400	18000	310	0.85	0.706	6.15	4.33	124.8

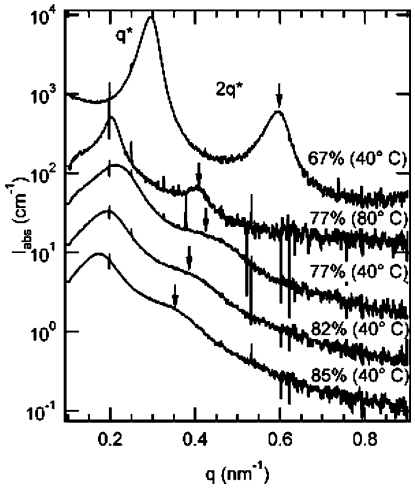

Figure 2. SAXS of PPV-*b*-PI block copolymers. SAXS indicates that all of the block copolymers are lamellar, as evidenced by the secondary peak or shoulder at $2q^*$ as indicated by arrows. The polymers become more disordered as coil fraction is increased, as evidenced by the decreased sharpness of the $2q^*$ peak. Annealing of PPVbPI-77 at a higher temperature leads to a sharpening of the scattering peaks, clearly demonstrating the lamellar structure.

blocks of the block copolymer may intermingle at the interface between the microdomains, and the domain size may fluctuate slightly as is expected in weakly segregated systems. These effects combine to produce a broad primary peak and diffuse second-order peak or shoulder (as marked by an arrow in Figure 2) typical of weakly ordered systems,[38] though the lamellar structure is still evident. For moderate coil fractions, annealing leads to a sharpening of the peaks, allowing the lamellar structure to be even more clearly determined. For compositions very close to the order−disorder composition, the higher order peaks never become well-defined, indicating a great deal of disorder in the samples.

As coil fraction is increased the structure remains lamellar, but the long-range order decreases rapidly as the order−disorder composition is approached, as seen in the TEM images shown in Figure 3. All of the polymers demonstrate stacks of several long parallel lamellae arranged in a polycrystalline morphology. Lamellae are characterized by little bending and a long persistence length, and grain boundaries are characterized by a breaking of the rod phase. Only the coil microphase is continuous. The amount of disorder in the lamellar structure increases as the coil fraction is increased, as evidenced by the shortened length of individual lamellae and a decreased correlation in the orientation of neighboring lamellae. For strongly asymmetric polymers which are very close to the order−disorder composition, clear grain boundaries and orientations are no longer apparent. The PPV-*b*-PI lamellae break through an increase in defects as the coil fraction is increased, and the TEM suggests that they form aggregates 100−200 nm long as they pass through the order−disorder composition. This transition appears to share some features with the body-centered-cubic sphere to the disordered micelle transition in coil−coil polymers.[39−41]

Liquid Crystalline Phase Transitions at High Coil Fractions. Upon heating, all of the samples transition from a microphase ordered to disordered state. The liquid crystallinity allows some of the polymers to retain alignment, corresponding to the nematic state beyond the disordering transition, as seen in Figure 1. The ODT temperature is identified by the disappearance of higher order Bragg reflections (peaks or shoulders) and by changes in the intensity of the primary peak. A detailed study of the peak intensity as a function of temperature for PPVbPI-67 (Figures 4 and 5) shows two clear transitions: the peak intensity decreases monotonically with increasing temperature until a point at which it becomes approximately constant, and the inverse peak intensity diverges with decreasing inverse temperature. The initial jump in $1/I$ occurs near 103 °C, and the leveling off of peak intensity occurs between 106 and 109 °C. The second-order peak disappears at 106 °C. Although the sharp discontinuity in intensity characteristic of the ODT in coil−coil block copolymers is not clearly observed,[42,43] both transitions in peak intensity and the disappearance of higher order peaks occur at the same temperature, providing a clear indication of the microphase order−disorder transition. The short plateau in peak intensity (Figure 4) from 94 to 100 °C may be a kinetic effect resulting from enhanced structural growth just below the ODT.[44] Similarly, the more pronounced increase in inverse intensity above the ODT may be a kinetic effect due to structural rearrangements within the nematic phase. The combination of divergence in inverse peak intensity and disappearance of higher order peaks is also used to determine the ODT of the other three polymers, as shown in Figure 5 and tabulated in Table 2. For more symmetric polymers the ODT temperature is comparable to that previously reported for similar molecular weights and coil fractions.[14] As coil fraction is increased, the ODT temperature drops rapidly. The sharp decrease in ODT with changing composition in highly asymmetric materials indicates the strong disordering effect of the coil and the ability to control thermal properties with small changes in composition.

Depending on the coil fraction of the polymer, further heating results in additional liquid crystalline transitions. Two distinct transition behaviors are observed, one where the lamellar block copolymer transitions first into a nematic disordered state, followed by an isotropic state at higher temperatures, and one where the lamellar phase transitions directly to an isotropic disordered state. DPLS curves (Figure 6) clearly demonstrate these two types of characteristic behavior. PPVbPI-67 displays behavior characteristic of block copolymers at lower coil fractions, where ordered, nematic, and isotropic phases are observed.[14] At low temperatures it has low transmission, high birefringence, and an optical pattern characteristic of smectic or layered phases by polarized optical microscopy (not shown). Heating results in an increase in transmission until the ODT is reached as confirmed by SAXS. As the polymer is heated further, the birefringence decreases, the transmission continues to increase, and a nematic texture is observed. Eventually the birefringence drops to zero, and the polymer loses all liquid crystalline texture under polarized optical microscopy, indicating the final transition into the isotropic phase. In this case, the

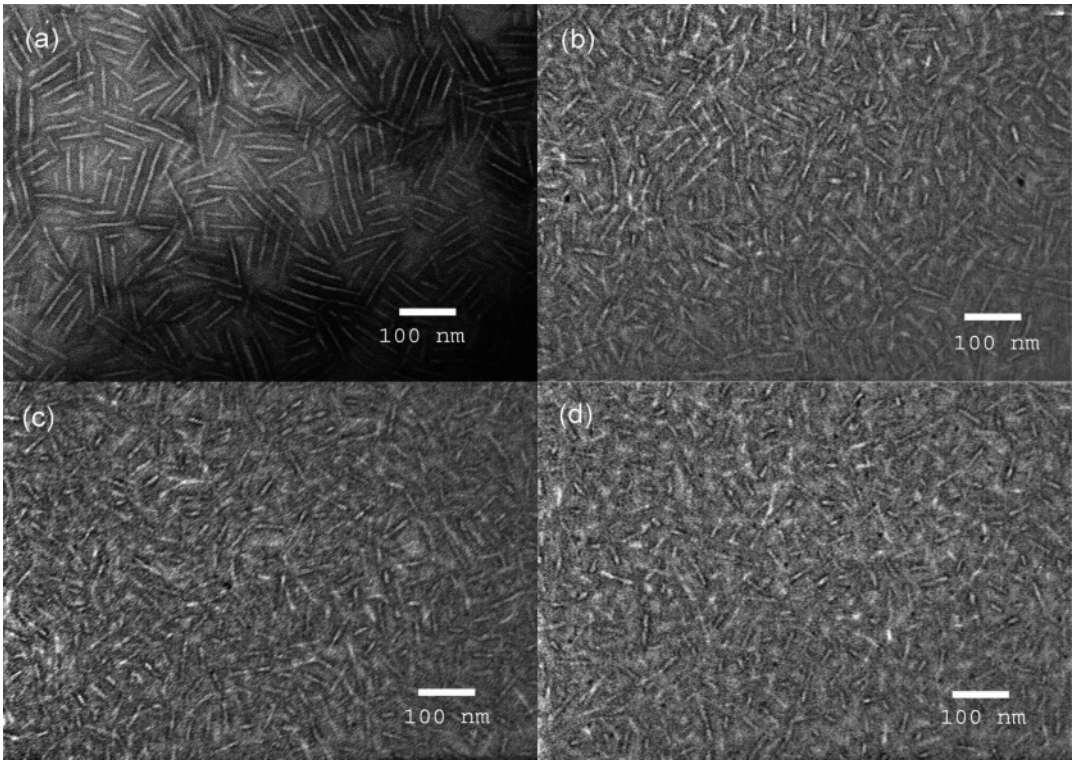

Figure 3. TEM of PPV-*b*-PI block copolymers. TEM demonstrates the increasing disorder of the lamellar structure with increasing coil fraction. At lower coil fractions, the polymers show well-ordered lamellar structure with long persistence lengths and defects characterized by breaks in the lamellae. Increasing the coil fraction results in an increasing degree of disorder in the lamellar structure. (a) PPVbPI-67, (b) PPVbPI-77, (c) PPVbPI-82, and (d) PPVbPI-85.

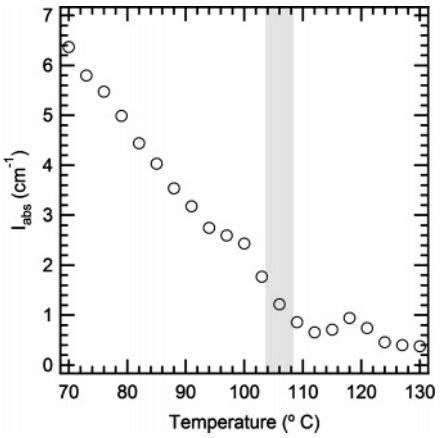

Figure 4. Determination of the order−disorder transition temperature based on primary peak intensity. Changes in primary peak intensity provide one method used to identify the ODT in rod−coil block copolymers. A gray band on the graph indicates the point at which the second-order peak disappears to within an error of ±3 °C. Peak intensity decreases as temperature is increased, and at the point where the second-order peak disappears there is a discontinuous change in slope. The inverse peak intensity shows a divergence at the same temperature. These results indicate that the disappearance of the second-order peak, change in the slope of intensity vs temperature, and divergence of the inverse peak intensity are all occur at similar temperatures and are indicative of the ODT.

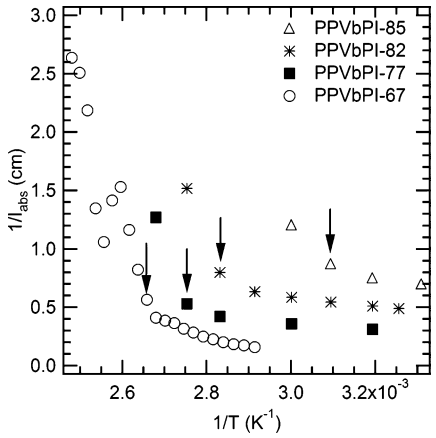

Figure 5. 1/*I* vs 1/*T* for the determination of the ODT. The ODT for each PPV-*b*-PI block copolymer is determined by the divergence of the inverse peak intensity in the 1/*I* vs 1/*T* plot and also by the disappearance of higher order peaks or shoulders. Arrows on the plot indicate the points at which the second-order peaks disappear. These points agree closely with the temperatures at which inverse intensities diverge, providing a clear indication of the ODTs. Curves are offset for clarity.

liquid crystalline clearing temperature corresponds to the nematic−isotropic transition. A second type of characteristic behavior is displayed by polymers with high coil fractions near the order−disorder composition. These polymers are weakly birefringent in the ordered phase, but no characteristic texture is observed by polarized optical microscopy even after long annealing times. The transmission steadily increases and birefringence steadily decreases with increasing temperature until birefringence drops to the baseline level at the liquid crystalline clearing temperature. The point at which birefringence disappears corresponds to the ODT in SAXS, so the polymer transitions directly from the ordered to isotropic phase. In this second case, the liquid crystalline clearing temperature corre-

Table 2. Thermal Transitions in Weakly Segregated Rod−Coil Block Copolymers (°C)

block copolymer	LC clearing temp (DPLS)	LC clearing temp (POM)	ODT
PPVbPI-67	134 ± 5	139 ± 3	106 ± 3
PPVbPI-77	95 ± 5	105 ± 3	90 ± 10
PPVbPI-82	81 ± 5	65 ± 3	80 ± 10
PPVbPI-85	54 ± 5		50 ± 10

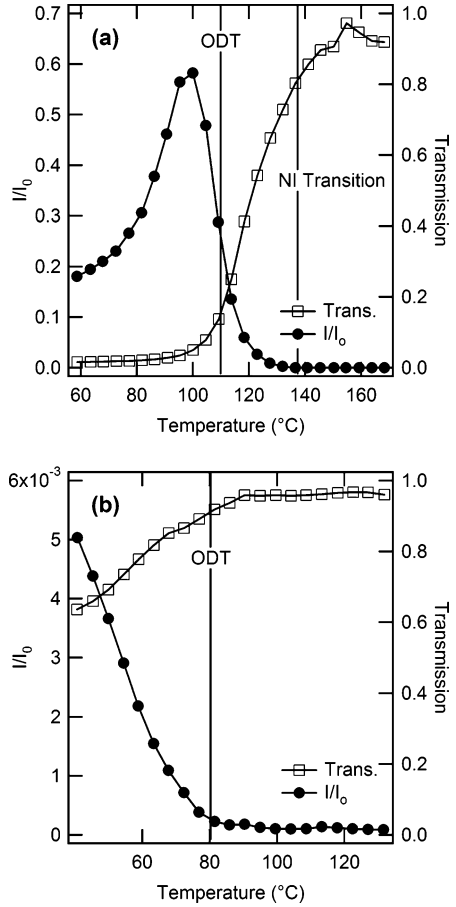

Figure 6. DPLS of PPV-*b*-PI block copolymers. Birefringence curves demonstrate the two characteristic disordering behaviors. (a) For polymers that are closer to symmetric (PPVbPI-67), both the microphase order−disorder and the nematic−isotropic transitions are observed. (b) At high coil fractions (PPVbPI-82), the polymer transitions directly from a lamellar to an isotropic as indicated by low birefringence that steadily decreases until it disappears at the ODT. The ODT marked on the above graphs was identified by SAXS, and the nematic−isotropic transition was identified by polarized optical microscopy.

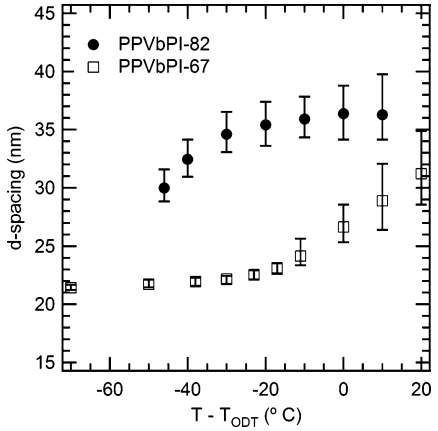

Figure 7. Changes in domain spacing in lamellar PPV-*b*-PI block copolymers. Heating PPV-*b*-PI block copolymers results in an increase in domain spacing, and the temperature at which domain spacing changes is dependent upon the liquid crystalline phase transition sequence. When the polymer passes through a nematic phase (low coil fractions: open markers), the domain spacing is constant below the ODT and then increases rapidly through the ODT and into the nematic phase. When the polymer undergoes a direct lamellar to isotropic transition (higher coil fractions: closed markers), the domain spacing increases below the ODT and then plateaus above it.

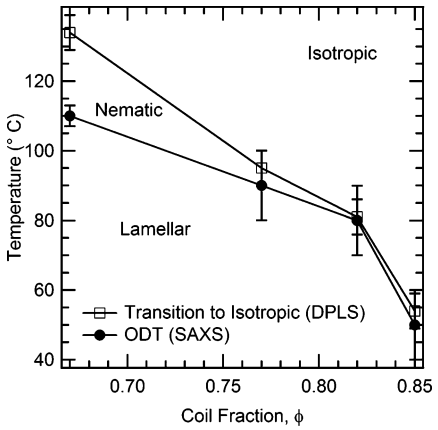

Figure 8. Phase diagram for PPV-*b*-PI at high coil fractions. The convergence of the liquid crystalline clearing temperature and the ODT is clear in this narrow region of phase space. For more symmetric polymers, the ordered phase transitions to a nematic and then isotropic phase upon heating, whereas for less symmetric polymers the ordered phase transitions directly into an isotropic disordered phase.

sponds to the lamellar−isotropic transition. As compared to PPVbPI-67, the birefringence signal of PPVbPI-82 is weak throughout the ordered regime, with a maximum I/I_0 roughly 2 orders of magnitude lower for the asymmetric polymers as compared to the symmetric polymers. Whereas the strong birefringence exhibited by symmetric polymers is characteristic of liquid crystalline materials, the weaker birefringent signal of the asymmetric polymers is more typical of the signal strength seen for traditional coil−coil lamellar block copolymers. The location of the transition to the isotropic phase is given in Table 2 for all of the polymers. Increasing coil fraction results in a sharp drop in the liquid crystalline clearing temperature from the rod homopolymer clearing temperature of 194 °C. Since the block molecular weight is constant throughout this study, the decrease in clearing temperature must be solely attributed to increasing coil fraction.

Changes in domain spacing with temperature also illustrate two types of behavior characteristic of the lamellar−nematic−isotropic and lamellar−isotropic transitions sequences (Figure 7), indicating that the characteristic size of the block copolymer is tied to the liquid crystalline phase. While all block copolymers show a counterintuitive increase in domain spacing upon heating, the nature of this increase depends on the liquid crystalline structure. The orienting forces present in liquid crystalline phases have the effect of stretching the block copolymers in the nematic phase, whereas block copolymers in the isotropic phase do not show this extension. As a result, the domain spacing in symmetric block copolymers remains constant in the lamellar phase and then increases rapidly as the polymer approaches the ODT and is heated into the nematic phase.[14] For polymers that disorder directly from a lamellar to an isotropic (coil fractions above ∼0.8), the domain spacing increases rapidly as the polymer is heated within the lamellar phase (below the ODT) and then levels off in the isotropic phase.

A more detailed phase diagram for asymmetric rod−coil block copolymers near the order−disorder composition is mapped out using the aggregate data from SAXS, TEM, DPLS, and polarized optical microscopy in Figure 8. The phase diagram clearly illustrates that at low coil fractions the polymers are characterized by transitions from lamellar to nematic to isotropic upon heating, whereas at higher coil fractions the polymers transition directly from lamellar to isotropic upon heating. The division between these two regimes occurs at a coil fraction of ∼0.8. Our experimental results are in qualitative agreement with the shape of the theoretical phase diagrams reported by Holyst

and Schick[15] and Reenders and ten Brinke.[16] Both of these theories predict isotropic phases at high temperature in systems with upper critical solution temperature (UCST) behavior. The experimentally observed transitions from an ordered phase to nematic and isotropic phases at low coil fraction and directly to an isotropic phase at high coil fraction are also predicted, and the predicted coil fraction dividing these two regimes is similar to that found experimentally. Pryamitsyn and Ganesan also predict these two transitional regimes using self-consistent-field theory.[12] They predict a relatively narrow nematic phase and a dividing point between the regimes at a lower coil fraction than experimentally observed, possibly due to differences between the parameter spaces probed in the experimental and theoretical studies. Despite qualitative similarities, quantitative comparison with these theories or estimation of the Flory−Huggins parameter based on the ODT temperature is not yet possible because experimental and theoretical studies have not yet matched the other three parameters in rod−coil phase space (coil fraction, Maier−Saupe parameter, and coil to rod length ratio).

Conclusions

A series of asymmetric weakly segregated model rod−coil block copolymers were studied near the ODT composition where small changes in either temperature or composition result in transitions between ordered, oriented, and disordered phases. Lamellar structures were observed across the entire range of coil fractions. The transition from an ordered lamellar to a disordered phase with increasing coil fraction is characterized by a gradual disordering of the lamellae rather than a change in microphase structure. The polymers show two phase transition regimes upon heating: one observed at lower coil fractions that is characterized by stable lamellar, nematic, and isotropic phases and a second at high coil fractions where polymers only demonstrate stable lamellar and isotropic phases. The transition between these two regimes occurs at a coil fraction of ∼0.8. The two sequences of phase transitions show qualitatively different birefringence and domain spacing behavior upon heating, suggesting the impact of a stable nematic phase on both optical properties and block copolymer conformation. The shape of the experimental phase diagram and the existence of these two transitional regimes agrees with theoretical predictions.

Acknowledgment. We gratefully acknowledge support from the ACS−Petroleum Research Fund and the Department of Energy Office of Basic Energy Sciences through the Plastic Electronics Program at Lawrence Berkeley National Lab (LBNL). SAXS experiments were performed at the Stanford Synchrotron Radiation Laboratory, a national user facility operated by Stanford University, and TEM experiments were performed at the National Center for Electron Microscopy at LBNL, both supported by the Department of Energy, Office of Basic Energy Sciences. We also thank John Pople for experimental assistance with SAXS and WAXS. B. D. Olsen gratefully acknowledges the Fannie and John Hertz Foundation for a graduate fellowship.

References and Notes

(1) Yu, G.; Gao, J.; Hummelen, J. C.; Wudl, F.; Heeger, A. J. *Science* **1995**, *270*, 1789−1791.
(2) Greenham, N. C.; Moratti, S. C.; Bradley, D. D. C.; Friend, R. H.; Holmes, A. B. *Nature (London)* **1993**, *365*, 628−630.
(3) Bates, F. S.; Fredrickson, G. H. *Phys. Today* **1999**, *52*, 32−38.
(4) Hamley, I. W. *The Physics of Block Copolymers*; Oxford University Press: New York, 1998.
(5) Fasolka, M. J.; Mayes, A. M. *Annu. Rev. Mater. Res.* **2001**, *31*, 323−355.
(6) Segalman, R. A. *Mater. Sci. Eng., R* **2005**, *48*, 191−226.
(7) Minich, E. A.; Nowak, A. P.; Deming, T. J.; Pochan, D. J. *Polymer* **2004**, *45*, 1951−1957.
(8) Osaheni, J. A.; Jenekhe, S. A. *J. Am. Chem. Soc.* **1995**, *117*, 7389−7398.
(9) Becker, S.; Ego, C.; Grimsdale, A. C.; List, E. J. W.; Marsitzky, D.; Pogantsch, A.; Setayesh, S.; Leising, G.; Mullen, K. *Synth. Met.* **2001**, *125*, 73−80.
(10) Yu, W. L.; Meng, H.; Pei, J.; Huang, W.; Li, Y. F.; Heeger, A. J. *Macromolecules* **1998**, *31*, 4838−4844.
(11) de Boer, B.; Stalmach, U.; van Hutten, P. F.; Melzer, C.; Krasnikov, V. V.; Hadziioannou, G. *Polymer* **2001**, *42*, 9097−9109.
(12) Pryamitsyn, V.; Ganesan, V. *J. Chem. Phys.* **2004**, *120*, 5824−5838.
(13) Matsen, M. W.; Barrett, C. *J. Chem. Phys.* **1998**, *109*, 4108−4118.
(14) Olsen, B. D.; Segalman, R. A. *Macromolecules* **2005**, *38*, 10127−10137.
(15) Holyst, R.; Schick, M. *J. Chem. Phys.* **1992**, *96*, 730−740.
(16) Reenders, M.; ten Brinke, G. *Macromolecules* **2002**, *35*, 3266−3280.
(17) Li, W. J.; Wang, H. B.; Yu, L. P.; Morkved, T. L.; Jaeger, H. M. *Macromolecules* **1999**, *32*, 3034−3044.
(18) Billot, J. P.; Douy, A.; Gallot, B. *Makromol. Chem., Macromol. Chem. Phys.* **1976**, *177*, 1889−1893.
(19) Billot, J. P.; Douy, A.; Gallot, B. *Makromol. Chem., Macromol. Chem. Phys.* **1977**, *178*, 1641−1650.
(20) Douy, A.; Gallot, B. *Polymer* **1987**, *28*, 147−154.
(21) Perly, B.; Douy, A.; Gallot, B. *Makromol. Chem., Macromol. Chem. Phys.* **1976**, *177*, 2569−2589.
(22) Lecommandoux, S.; Achard, M. F.; Langenwalter, J. F.; Klok, H. A. *Macromolecules* **2001**, *34*, 9100−9111.
(23) Chen, J. T.; Thomas, E. L.; Ober, C. K.; Hwang, S. S. *Macromolecules* **1995**, *28*, 1688−1697.
(24) Chen, J. T.; Thomas, E. L.; Ober, C. K.; Mao, G. P. *Science* **1996**, *273*, 343−346.
(25) Li, C. Y.; Tenneti, K. K.; Zhang, D.; Zhang, H. L.; Wan, X. H.; Chen, E. Q.; Zhou, Q. F.; Carlos, A. O.; Igos, S.; Hsiao, B. S. *Macromolecules* **2004**, *37*, 2854−2860.
(26) Radzilowski, L. H.; Wu, J. L.; Stupp, S. I. *Macromolecules* **1993**, *26*, 879−882.
(27) Radzilowski, L. H.; Stupp, S. I. *Macromolecules* **1994**, *27*, 7747−7753.
(28) Radzilowski, L. H.; Carragher, B. O.; Stupp, S. I. *Macromolecules* **1997**, *30*, 2110−2119.
(29) Lee, M.; Oh, N. K.; Lee, H. K.; Zin, W. C. *Macromolecules* **1996**, *29*, 5567−5573.
(30) Lee, M.; Oh, N. K. *J. Mater. Chem.* **1996**, *6*, 1079−1086.
(31) Lee, M.; Cho, B. K.; Kim, H.; Yoon, J. Y.; Zin, W. C. *J. Am. Chem. Soc.* **1998**, *120*, 9168−9179.
(32) Ryu, J. H.; Oh, N. K.; Zin, W. C.; Lee, M. *J. Am. Chem. Soc.* **2004**, *126*, 3551−3558.
(33) Gopalan, P.; Zhang, Y. M.; Li, X. F.; Wiesner, U.; Ober, C. K. *Macromolecules* **2003**, *36*, 3357−3364.
(34) Kretzschmann, H.; Meier, H. *Tetrahedron Lett.* **1991**, *32*, 5059−5062.
(35) Ortega, A.; de la Torre, J. G. *J. Chem. Phys.* **2003**, *119*, 9914−9919.
(36) Riseman, J.; Kirkwood, J. G. *J. Chem. Phys.* **1950**, *18*, 512−516.
(37) Garetz, B. A.; Newstein, M. C.; Dai, H. J.; Jonnalagadda, S. V.; Balsara, N. P. *Macromolecules* **1993**, *26*, 3151−3155.
(38) Roe, R.-J. *Methods of X-Ray and Neutron Scattering in Polymer Science*; Oxford University Press: New York, 2000.
(39) Han, C. D.; Vaidya, N. Y.; Kim, D.; Shin, G.; Yamaguchi, D.; Hashimoto, T. *Macromolecules* **2000**, *33*, 3767−3780.
(40) Wang, X. H.; Dormidontova, E. E.; Lodge, T. P. *Macromolecules* **2002**, *35*, 9687−9697.
(41) Schwab, M.; Stuhn, B. *Phys. Rev. Lett.* **1996**, *76*, 924−927.
(42) Sakamoto, N.; Hashimoto, T. *Macromolecules* **1995**, *28*, 6825−6834.
(43) Bates, F. S.; Rosedale, J. H.; Fredrickson, G. H. *J. Chem. Phys.* **1990**, *92*, 6255−6270.
(44) Kim, W. G.; Garetz, B. A.; Newstein, M. C.; Balsara, N. P. *J. Polym. Sci., Part B: Polym. Phys.* **2001**, *39*, 2231−2242.

MA060994Z